VINTERGATAN IV: Cosmic phases of star formation in Milky Way-like galaxies

Álvaro Segovia Otero,[★] Florent Renaud, and Oscar Agertz
Department of Astronomy and Theoretical Physics, Lund Observatory, Box 43, SE-221 00 Lund, Sweden

20 June 2022

ABSTRACT

The star formation history of a galaxy is modulated by a plethora of internal processes and environmental conditions. The details of how these evolve and couple together is not fully understood yet. In this work, we study the effects that galaxy mergers and morphological transformations have on setting different modes of star formation at galactic scales and across cosmic time. We monitor the global properties of VINTERGATAN, a 20 pc resolution cosmological zoom-in simulation of a Milky Way-type galaxy. Between redshifts 1 and 5, we find that major mergers trigger multiple starburst episodes, corresponding to a tenfold drop of the gas depletion time down to 100 Myr. Bursty star formation is enabled by the emergence of a galactic disc, when the rotational velocity of gas starts to dominate over its velocity dispersion. Coherent motions of gas then outweigh disordered ones, such that the galaxy responds to merger-induced forcings by redistributing large amounts of gas towards high densities. As a result, the overall star formation rate is enhanced with an associated decrease in the depletion time. Before redshift 5, mergers are expected to be even more frequent. However, a more turbulent interstellar medium, is incapable of reacting in such a collective manner so as to spark rapid star formation. Thus, a constant long depletion time of 1 Gyr is kept, along with a low, but gradually increasing star formation rate. After the last major merger at redshift 1, VINTERGATAN spends the next 8 Gyr evolving secularly. It has a settled and adiabatically growing disc, and a constant star formation rate with gas depletion times of 1-2 Gyr. Our results are compatible with the observed rapid transition between different modes of star formation when galaxies leave the main sequence.

Key words: galaxies: interactions – galaxies: starburst – methods: numerical

1 INTRODUCTION

Understanding star formation is a multi-scale, multi-physics problem and one of the main challenges in modern astrophysics. Over the last couple of decades, catalogues of extragalactic sources based on CO line fluxes, millimeter dust photometry, and far-infrared dust emission have enable the study of star formation properties across cosmic time (e.g. Tacconi et al. 2020; Saintonge & Catinella 2022, and references therein). One of the major statistical conclusions stemming from such a wealth of data is that most star-forming galaxies up to $z \approx 6$ lie on the so called "main sequence" of star formation (hereafter MS, Noeske et al. 2007; Elbaz et al. 2007, 2011; Genzel et al. 2010; Whitaker et al. 2014; Tacconi et al. 2013; Saintonge et al. 2017). The MS correlates star formation rates (SFR) and stellar masses ($M_\star$), and evolves as a function of cosmic time. Galaxies on the MS formed stars at higher rates (per unit of stellar mass) in the earlier Universe, being affected by different gas accretion and assembly histories (Whitaker et al. 2012). Hence, it is remarkable that at a given stellar mass and redshift, the scatter of the MS is small ($0.2 - 0.4$ dex, see Speagle et al. 2014, and references therein).

MS galaxies are mostly blue in rest-frame $U - V$ bands (Brinchmann et al. 2004; Vilella-Rojo et al. 2021), commonly host rotationally-supported discs with $v_{\rm rot,gas}/\sigma_{\rm gas} > 1$ (Wisnioski et al.

2015; Jones et al. 2021; Fraser-McKelvie et al. 2021), and feature Sérsic indices of $n \approx 1 - 2$ (Wuyts et al. 2011; Lang et al. 2014; Osborne et al. 2020). Their gas reservoirs change with time following the normalisation of the MS, with gas fractions ranging from 10% in the local Universe (Leroy et al. 2008) up to 60% at $z \approx 4$ (Tacconi et al. 2010). This indicates a strong connection between gas and SFRs, well-known for most MS galaxies, but not fully understood in detail.

The Kennicutt-Schmidt relation (hereafter KS, Schmidt 1959; Kennicutt 1998) is an empirical result showing the dependency between surface densities of gas and SFR as $\Sigma_{\rm SFR} \propto \Sigma_{\rm gas}^n$. Discs in this diagram broadly follow the so-called canonical KS relation, with $n \approx 1.4$ (Kennicutt & Evans 2012). The depletion time, $\tau_{\rm dep} = \Sigma_{\rm gas}/\Sigma_{\rm SFR} = M_{\rm gas}/{\rm SFR}$, provides a timescale for star formation: discs along the MS spanning masses of $9 < M_\star/{\rm M_\odot} < 12$ have, on average, $\tau_{\rm dep} \approx 0.5 - 2$ Gyr (e.g. Wang et al. 2022), with a moderate decrease of up to $z \approx 3$ (Genzel et al. 2015; Tacconi et al. 2018). This means that smooth continuous accretion of gas is required to sustain star formation throughout the lifetime of a galaxy.

Starburst galaxies are in stark contrast with this dominant mode of star formation, and are characterised as out-of-equilibrium systems with intense star formation activity on timescales of $10 - 500$ Myr (Pan et al. 2018; Birkin et al. 2021). Either because of an enhanced $\Sigma_{\rm SFR}$, reduced $\Sigma_{\rm gas}$, or a combination of both, starburst galaxies make a separate trend in KS space with significant drops in $\tau_{\rm dep}$

(Daddi et al. 2010b; Rodighiero et al. 2011). They present enhanced SFRs per unit mass, but can also be found within the scatter of the MS (Puglisi et al. 2021; Gómez-Guijarro et al. 2022). In the local Universe, they generally correspond to luminous and ultra-luminous infrared galaxies (LIRGs and ULIRGs) powered by ongoing wet major mergers (Kim et al. 2021). However, moving to higher redshifts ($z > 1$), correlating short-lived bursts of star formation with galaxy interactions becomes a difficult task. Starbursts only contribute ~5% to the cosmic SFR density. While their fraction appears to be constant with time (Sargent et al. 2012; Schreiber et al. 2015; Hani et al. 2020), the merger rate is a continuously increasing function of redshift (Lotz et al. 2011; Duncan et al. 2019, see also Romano et al. 2021; Huško et al. 2022 for merger rates of massive galaxies). Thus, it is of utter importance to investigate how the galactic gas reservoir responds to merger events at different cosmic epochs.

Large-scale cosmological simulations attempt to explain the mechanisms driving starbursts by reproducing the MS, the KS relation, and their outliers. They face two important issues. First, low spatial (~100 pc) and gas mass ($> 10^6$ M$_\odot$) resolutions lead to a recovered starburst contribution of barely 1% of the total SFR density (Vogelsberger et al. 2014; Sparre et al. 2015). Second, the choice of sub-grid models to describe the impact of feedback, turbulence, and star formation on the structure of the interstellar medium (ISM) significantly influences the outcome of simulations (Agertz et al. 2013; Hopkins et al. 2013; Sparre et al. 2017). With improved spatial ($10 - 100$ pc) and gas mass (10^5 M$_\odot$) resolutions, recent simulations retrieve realistic starburst fractions (e.g. Rodríguez Montero et al. 2019; Nelson et al. 2021). Now, idealised isolated merger simulations (Hopkins et al. 2018; Moreno et al. 2021) disentangle the building blocks of a standardised merger-induced starburst picture: interacting galaxies can exert torques that globally channel gas towards the centre, compress it into higher surface densities, and spark nuclear starbursts (Keel et al. 1985). With spatial and mass resolution on the order of parsecs and ~10^3 M$_\odot$ respectively, they are also capable of tracking how the local turbulent and density structures of the ISM affect star formation. Renaud et al. (2014) and Sparre & Springel (2016) register merger-driven SFR enhancements and tenfold declines in $\tau_{\rm dep}$. Renaud et al. (2014) established the link between gravitational interactions and the local turbulence properties and gas probability density functions (PDFs) of the ISM. Compressive tides and turbulence translate the global merger-driven forcing into boosted galactic star formation over large volumes. Both nuclear and off-centered starbursts are reproduced from an excess of high density gas. Nevertheless, a consistent view including the full cosmological context of a galaxy is still missing (specially at high redshift where high gas fractions blur the picture of this coupling, see e.g. Perret et al. 2014; Fensch et al. 2017).

In this work we use VINTERGATAN, a 20 pc resolution cosmological zoom-in simulation of a Milky Way-like galaxy, to study how the evolution of the cosmological environment and properties of the ISM lead to different phases of star formation. The layout of the paper is the following: Section 2 briefly summarises the simulation setup; Section 3 shows how the starburst activity is associated with both mergers and disc formation; Section 4 first lists the main conclusions and then discusses the implications of this work.

2 METHOD

This work uses the VINTERGATAN cosmological zoom-in simulation (Agertz et al. 2021; Renaud et al. 2021a,b, hereafter Paper I; Paper

II; Paper III). A brief summary of the numerical recipe is provided below, with a more detailed description in Paper I.

The simulation was run using RAMSES (Teyssier 2002), a hydrodynamic+N-body code with adaptive mesh refinement. Its initial conditions are the same as those of "m12i" from Hopkins et al. (2014), i.e. a virial[1] radius of $R_{200,m} = 334$ kpc and a virial mass of $M_{200,m} = 1.3 \times 10^{12}$ M$_\odot$ at $z = 0$. Within a cosmological box of 85 Mpc containing 512^3 particles, a zoom-in technique (Hahn & Abel 2011) is applied to the progenitor halo, achieving resolutions of 3.5×10^4 M$_\odot$ for dark matter, 7070 M$_\odot$ for gas, and a physical resolution of ~20 pc in the dense ISM. We stopped the simulation at $z \approx 0.17$ (2.1 Gyr), due to computational costs and because the galaxy was not evolving significantly passed this redshift. The result is a Milky Way-type galaxy of ~7×10^{10} M$_\odot$ in stellar mass and ~10^{10} M$_\odot$ in gas.

Star formation is modelled as a Poisson process, where star particles of 10^4 M$_\odot$ are generated on a cell-by-cell basis following the law

$$\dot{\rho}_\star = \epsilon_{\rm ff} \frac{\rho_{\rm gas}}{t_{\rm ff}} \quad \text{with} \quad \rho_{\rm gas} > 100\,{\rm cm}^{-3} \quad \text{and} \quad T_{\rm gas} < 100\,{\rm K}. \quad (1)$$

Here, $\dot{\rho}_\star$ is the star formation rate density, $t_{\rm ff}$ is the local free-fall time and $\epsilon_{\rm ff}$ is the local star formation efficiency per free-fall time, parametrised according to Padoan et al. (2012). These star particles represent individual stellar populations with stellar feedback processes including stellar winds, radiation pressure, type II, and type Ia supernovae (Agertz et al. 2013; Agertz & Kravtsov 2015, 2016).

Cooling is metallicity-dependent and adopted from Sutherland & Dopita (1993) for $T > 10^4$ K, and Rosen & Bregman (1995) for $T < 10^4$ K. An initial gas metallicity floor is set to 10^{-3} Z$_\odot$ to reproduce the enrichment from unresolved population III stars (Wise et al. 2012). Also accounted for is the additional gas heating from the ultraviolet background radiation field (Haardt & Madau 1996) assuming a reionization epoch at $z = 8.5$.

3 RESULTS

As demonstrated in Paper I, VINTERGATAN reproduces key observational results on the formation of the Milky Way, including the chemical bimodality in [α/Fe]-[Fe/H], the thin-thick disc dichotomy, and the similarity of the surface brightness and rotational velocity profiles with that of nearby disc galaxies. Therefore, our simulated galaxy sets realistic grounds for studies of the physics of star formation in Milky Way-like galaxies and their progenitors.
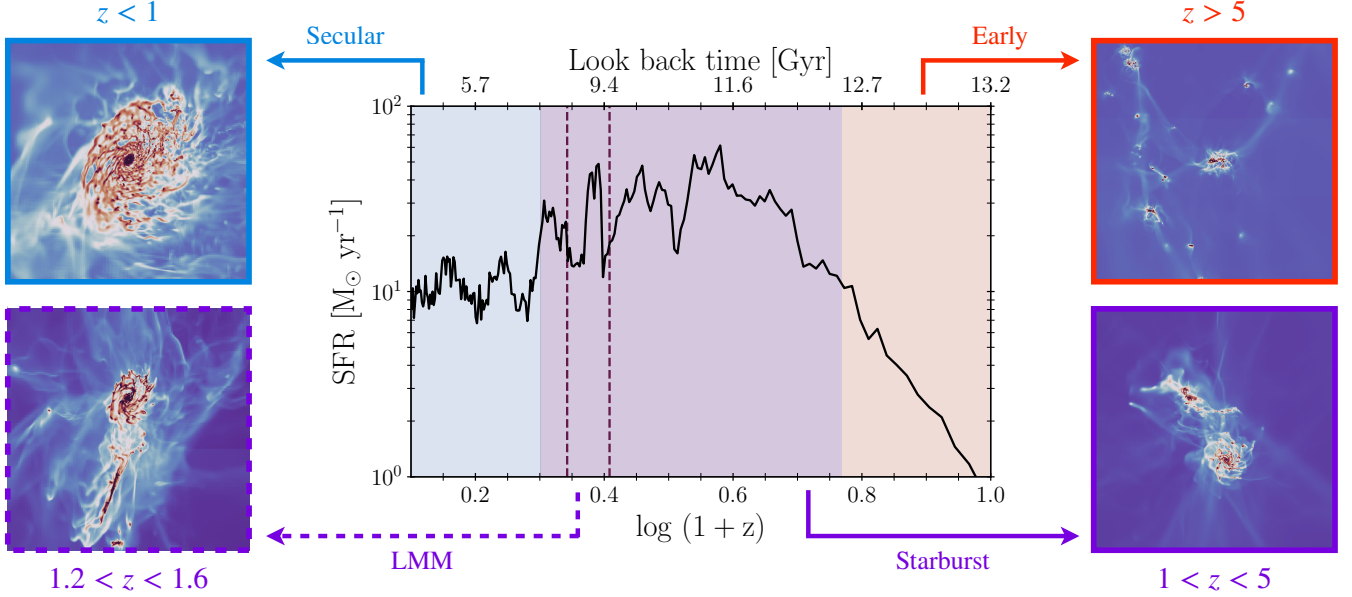
3.1 Star formation history

Figure 1 shows the star formation history of VINTERGATAN, calculated including all stars in the last snapshot ($z \approx 0.2$, 2.2 Gyr ago) within a sphere of radius $3R_{1/2}$[2], and arranged in age bins of 150 Myr. From right to left in Figure 1, we define three distinct phases:

a) *Early* ($z > 4.8$, 12.7 Gyr ago): VINTERGATAN is slowly, but steadily increasing its SFR of a few M$_\odot$ yr^{-1}. Our small compact gas-rich galaxy is therefore smoothly building its stellar mass ($R_{1/2} \approx 1$ kpc,

---

[1] This value is measured at $\Delta = 200$ with respect to the mean cosmic background density.

[2] $R_{1/2}$ is computed for the most massive progenitor of VINTERGATAN for each snapshot, as the half-mass radius of stars younger than 100 Myr (see Paper II).

Figure 1. Star formation history of VINTERGATAN. The plot is colour-coded to highlight three epochs in chronological order (from right to left): *Early* (orange), *Starburst* (purple), and *Secular* (blue). The vertical dashed lines mark the first pericenter passage ($z \approx 1.6$) and the final coalescence ($z \approx 1.2$) of the last major merger. An illustrative thumbnail 40 kpc wide shows the projected gas density at each evolutionary stage. During the *Starburst* phase, as opposed to the *Early* and *Secular* ones, the SFR reaches several short-lived maxima above $40 \, M_\odot \, yr^{-1}$.

$M_\star < 10^9 \, M_\odot$, $f_{gas} \gg 50\%$). Mergers are frequent and prevent the development of an ordered morphology (Paper II). In spite of the elevated rate of galaxy interactions, no starburst activity exists at this stage.

b) *Starburst* ($1 < z < 4.8$, $7.8 - 12.7$ Gyr ago): the galaxy transitions into a phase still merger-dominated, but much more active in terms of star formation. In the span of 5 Gyr, VINTERGATAN experiences four major merger events that give rise to SFR peaks of $\sim 40 \, M_\odot \, yr^{-1}$ (Paper II).

c) *Secular* ($z < 1$, 7.8 Gyr ago): comparing the top left and bottom left thumbnails in Figure 1 shows that after the last major merger (LMM, coalescence at $z \approx 1.2$), VINTERGATAN settles into a massive and extended disc ($R_{1/2} \approx 4.8$ kpc, $M_\star \approx 10^{11} \, M_\odot$, $f_{gas} \approx 10 - 20\%$, Paper I). Its SFR has moderate oscillations of $\sim 3 \, M_\odot \, yr^{-1}$ when minor satellites accrete onto the main galaxy. Both $M_\star$ and the SFR are compatible with that of observed MS discs at these redshifts (Whitaker et al. 2012; Speagle et al. 2014).

This first diagnostic suggests that mergers are a necessary but not sufficient condition to boost the SFR. Although the merger rate decreases with z (as inferred statistically from observations, e.g. Rodighiero et al. 2011; Schreiber et al. 2015, and simulations, e.g. Fakhouri et al. 2010), intense phases of star formation only occur between redshifts 1 and 5. Since the environment of VINTERGATAN in both the *Early* and *Starburst* epochs is similar in terms of interactions, we suspect that structural modifications in the ISM are responsible for the different modes of star formation. This is explained in Section 3.5.

3.2 The Kennicutt-Schmidt relation

The evolution of a galaxy in the KS diagram evaluates to what degree it is undergoing a starburst episode, provided a control sample. Galaxies in Figure 2 can be grouped in two categories: those along

the canonical KS relation, also referred to as the "disc sequence" (solid line), and the "starburst sequence" (dotted line), shifted ~ 1 dex above the disc sequence. High redshift gas-rich galaxies on the disc sequence have increased Σ_{SFR} and Σ_{gas} compared to local discs, with only a slight decrease in τ_{dep} (Daddi et al. 2010a), whereas galaxies on the starburst sequence feature a significantly lower τ_{dep} (Daddi et al. 2010b; Rodighiero et al. 2011).

For VINTERGATAN, Σ_{gas} and Σ_{SFR} are calculated on each simulation snapshot by accounting for the mass of cold gas ($T < 10^4$ K) and stars younger than 100 Myr. Both quantities are computed within a sphere of radius $3R_{1/2}$. The evolution of VINTERGATAN in Figure 2 shows that the galaxy resides in the disc sequence in the *Early* phase, jumps onto the starburst sequence during the *Starburst* phase, and returns back to the disc sequence in the *Secular* phase, consistent with nearby discs in the THINGS survey (Bigiel et al. 2008). Contrarily to observations that usually select interacting galaxies near their peak of star formation activity, our stacked outputs include moments of quiescence in between mergers, which reduces the average value of Σ_{SFR} and Σ_{gas} shown here.

3.3 Depletion time across cosmic time

In Figure 3, we trace the evolution of τ_{dep} in VINTERGATAN and compare it to observed data of star-forming galaxies from the PHIBSS survey (Tacconi et al. 2018). In the *Secular* phase (blue shaded region), the depletion time of our simulated galaxy varies between $1 - 2$ Gyr. This is in agreement with observations of the nearby galaxies in Leroy et al. (2013), but PHIBSS galaxies display higher SFRs at similar gas masses, leading to systematically lower τ_{dep}. In the *Starburst* epoch (comprising several major mergers, purple shaded region), τ_{dep} repeatedly drops to 100 Myr. The general trend of our simulation is consistent with the PHIBSS data, but the latter shows a slight decline of a factor of ~ 3 up to $z \approx 4.5$. The regularity of the PHIBSS curve is a consequence of stacking, which emphasises
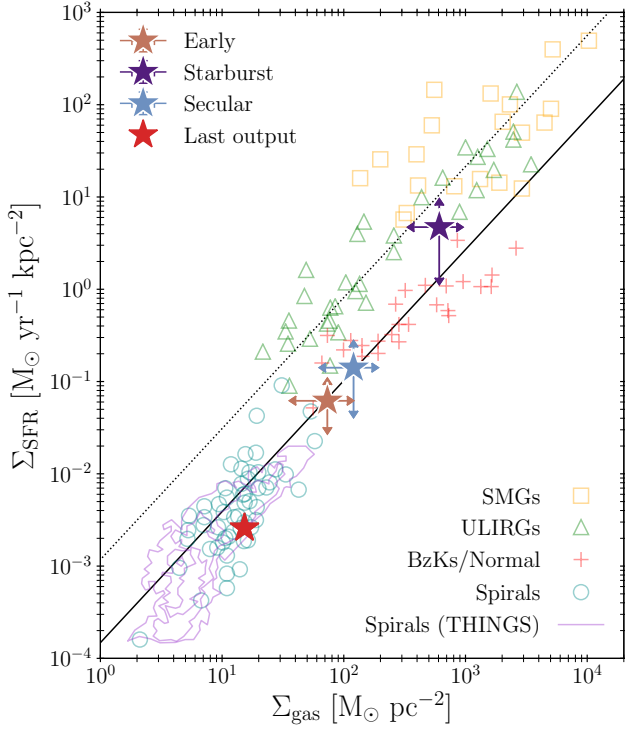
Figure 2. KS relation comparing observations of extragalactic sources (bottom right legend) with VINTERGATAN (top left legend). Observations comprise sub-millimeter galaxies at $1.4 < z < 3.4$ (SMGs, Bouché et al. 2007; Bothwell et al. 2009), ULIRGs at low redshift (Kennicutt 1998), BzKs at $z \approx 1.5$ (Daddi et al. 2010a), normal galaxies at $1 < z < 2.3$ (Tacconi et al. 2010), spiral galaxies (Kennicutt 1998), and spirals from the THINGS survey (Bigiel et al. 2008). Star markers indicate the location of VINTERGATAN on this plane, with values averaged over all snapshots corresponding to each phase identified in Figure 1. The *Secular* regime includes 36 stacked snapshots, 33 in *Starburst*, and 7 *Early*. The arrows indicate the $\pm 0.5\sigma$ standard deviations. Along its lifetime, the galaxy transitions from the disc sequence (solid line) and reaches the starburst sequence (dotted line, Equation 2 in Daddi et al. 2010b) during its *Starburst* phase, before coming back to the disc sequence.

the statistically significant behaviour of a large sample of galaxies as a function of redshift. Stacking smooths out the fluctuations from individual galaxies like VINTERGATAN, with more abrupt dips in τ_{dep} due to mergers.

One of the major sources of uncertainty in deriving τ_{dep} from observations is the CO-to-H_2 conversion factor. For instance, α_{CO} translates the CO emission intensity into the total mass of H_2. α_{CO} is observed to fluctuate with the galactic environment, e.g. between isolated disc galaxies and mergers (Bolatto et al. 2013). The underlying reasons are however debated. Based on predictions from simulations, Renaud et al. (2019a) propose a model to adjust α_{CO} as a function of the stage of a merger, such that a reduced α_{CO} is expected when the galaxy hosts a starburst. By applying this model to the τ_{dep} of all the PHIBSS galaxies, we find that τ_{dep} would change by a factor less than 2, at $z > 1$. Nevertheless, this effect happens to be comparable to or even smaller than the scatter in α_{CO} due to the use of different CO lines for each galaxy (see Appendix A).

A striking result from Figure 3 is the long τ_{dep} during the *Early* phase, despite the merger activity. At this epoch, the galaxy forms stars with depletion times of ~1 Gyr. This is ten times slower than in
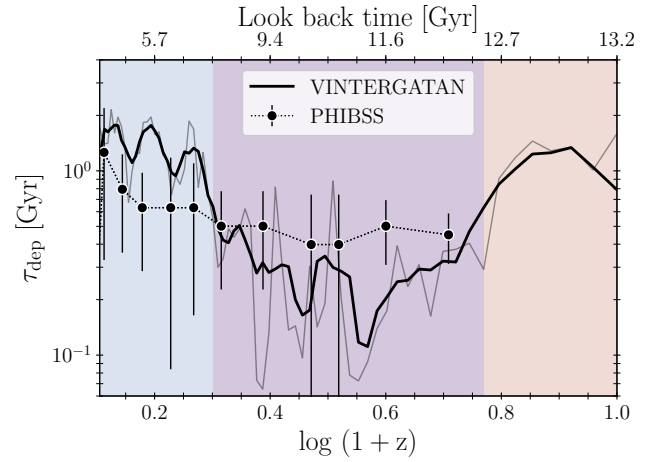
Figure 3. Cosmic evolution of τ_{dep} in VINTERGATAN in solid grey, smoothed for clarity in black. We also show the median of the depletion times of galaxies in the PHIBSS survey (Tacconi et al. 2018) divided in 30 redshift bins in logarithmic scale covering $0.003 < z < 4.5$. The error bars represent the median absolute deviation (MAD = 0.67449σ, Müller 2000). The coloured regions follow the same coding as in Figure 1. Overall, τ_{dep} drops by an order of magnitude in the *Starburst* epoch with respect to the *Secular* and *Early* ones.

the *Starburst* epoch. These changes in depletion time reflect modifications of the density structure of the ISM, as shown below.
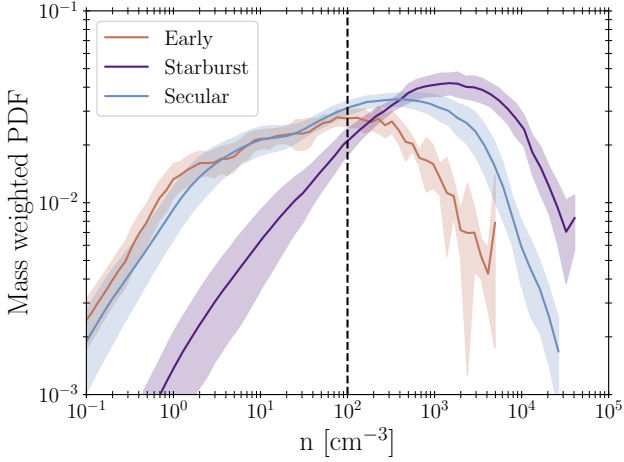
3.4 Gas density PDFs

According to turbulence theory of isothermal supersonic gas, the density PDF of the ISM follows a log-normal functional form (Federrath et al. 2010). For isolated disc simulations, log-normal distributions provide a good fit, even with a non-isothermal ISM (Robertson & Kravtsov 2008; Renaud et al. 2013). The gas density PDF is sensitive to the volume over which it is measured. This is particularly important in cosmological simulations, where inflows, outflows and incoming galaxies can modify the shape of the PDF, specially at its low-density end. This blurs the information on local turbulence properties conveyed by the PDF.

We focus on understanding whether the evolution of τ_{dep} in our three phases corresponds to variations in the shape of the density PDFs (Figure 4). In comparison with the *Secular* phase, the PDF in the *Starburst* epoch shows an excess of gas at high densities. During this epoch, large amounts of gas are compressed into dense star-forming states, leading to rapid star formation events, i.e. short τ_{dep}. In idealised simulation of mergers, the excess of dense gas and the reduction of the depletion time have been associated with tidal compression (Renaud et al. 2009, 2014, 2019b). This is also the case in cosmological context (see Renaud et al. in prep.). This is why VINTERGATAN jumps to the starburst regime in the KS plane, rather than moving along the canonical relation. We stress that this conclusion is independent of any uncertainty on α_{CO} (Figure 2).

Conversely, the gas in the *Early* phase does not reach such dense states in spite of VINTERGATAN interacting with neighbour galaxies. This suggests a shift in the structure of the ISM between the *Early* and *Starburst* phases.

Figure 4. Gas density PDFs of VINTERGATAN. For each phase, the PDFs show the normalized distribution of mass-weighted densities, averaged over the same number of stacked snapshots per cosmic epoch as in Figure 2. The shaded regions delimit the $\sigma/3$ region, and the vertical dashed line marks the threshold for star formation (Equation 1). The *Starburst* phase (when the galaxy experiences rapid star formation episodes, i.e. low τ_{dep} caused by major mergers) shows an excess of gas at high densities.
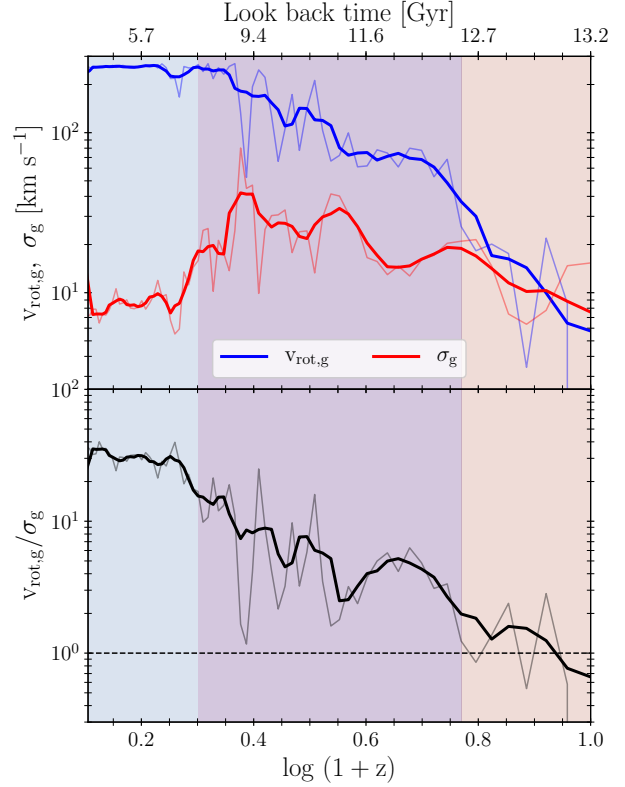
3.5 Disc assembly

Gas kinematics is a robust tracer of disc assembly, with high-quality observations characterising the dynamical state of a large sample of galaxies across cosmic time, (e.g. Wisnioski et al. 2019; Rizzo et al. 2021). Studies in this field commonly use the gas rotational velocity $v_{rot,g}$ to quantify organised circular motions, and the velocity dispersions σ_g for the turbulent behaviour of the gas. One can consider that the disc is in place when $v_{rot,g}/\sigma_g > 1$, i.e. when circular motions dominate turbulent ones.

For every snapshot, we compute the rotation axis of the main progenitor galaxy as the total angular momentum vector of the cold gas ($T < 10^4$ K) within $3R_{1/2}$. We then split the enclosed volume into a grid of $(100\,\text{pc})^3$ bins and, to ensure statistical significance, we evaluate the $v_{rot,g}/\sigma_g$ ratio only in those bins that contain more than 10 cold gas cells. For $v_{rot,g}$, we use the modulus of the tangential velocity in cylindrical coordinates. We calculate σ_g at 100 pc scale via $\sigma_g^2 = (\sigma_x^2 + \sigma_y^2 + \sigma_z^2)/3$, where σ_i represents the standard deviation of each component of the total gas velocity $\vec{v}_g$.

Each point shown in Figure 5 corresponds to the median value of these bins for each output of the simulation. Throughout the *Secular* phase, we see a steep decline of σ_g with decreasing redshift from ~40 km s^{-1} to <10 km s^{-1}, along with a rather constant rotational velocity above ~200 km s^{-1}. This is a strong indication of disc settling (Paper III), consistent with the kinematic downsizing picture of Kassin et al. (2012) and Simons et al. (2017). In the *Starburst* phase, the presence of ongoing interactions (and the associated starburst and stellar feedback) sustain a high σ_g with a remarkable increase in $v_{rot,g}$ with decreasing redshift. Despite such a violent environment, the $v_{rot,g}/\sigma_g$ ratio stays above unity.

In the earliest epochs ($z > 4.8$), the morphology of the galaxy is complex. Computing the angular momentum vector of this object leads to fluctuating orientations of the rotation axis and therefore substantially different values of the rotational velocities. This, together with velocity dispersions of comparable amplitude as $v_{rot,g}$, indicates that coherent and disordered motions are of the same order

Figure 5. *Top:* Rotational velocity $v_{rot,g}$ (blue) and velocity dispersion σ_g (red) of the cold gas as a function of redshift in VINTERGATAN; *Bottom:* $v_{rot,g}/\sigma_g$ ratio, used to parametrise disc assembly with cosmic time. All three curves have been smoothed in the same way as in Figure 3, and the shaded regions are coloured following the same code as in Figure 1. The transition at $\log(1+z) \approx 0.75$ (i.e. $z \approx 4.8$, 12.5 Gyr ago) initiates the formation of a galactic disc, coeval with an excess of dense gas causing a drop in τ_{dep} and the onset of starbursts (Figures 3 and 4). A more rotationally-supported disc settles after the LMM with $v_{rot,g}/\sigma_g > 10$ at $\log(1+z) \approx 0.3$ (i.e. $z \approx 1.2$, 8.5 Gyr ago).

of magnitude ($v_{rot,g} \approx \sigma_g$). According to the kinematic downsizing scenario (Kassin et al. 2012; Simons et al. 2017), the formation of a galactic disc for a Milky Way progenitor ($M_\star \sim 10^9$ M$_\odot$) is unlikely before $z \approx 5$. Mergers, gas accretion from counter-rotating streams, stellar feedback and violent disc instabilities during this period allude to high-redshift galaxies with large $v_{rot,g}/\sigma_g$ as rare objects. Yet, this has been questioned by the recent detections of Neeleman et al. (2020); Rizzo et al. (2020); Fraternali et al. (2021); Lelli et al. (2021). These massive ($M_\star \gtrsim 10^{10}$ M$_\odot$), dusty, starburst discs at $z > 4$ have rotational velocities of the order of hundreds km s^{-1}, and 10 times lower velocity dispersion. Long-lived discs at high redshift can also be reproduced in simulations if galaxies are massive and isolated enough, where filamentary accretion of gas with high angular momentum is co-planar and aligned with the disc (Dekel et al. 2020; Tamfal et al. 2021; Kretschmer et al. 2022). Despite VINTERGATAN being an order of magnitude less massive than the aforementioned objects and hosting more modest rotational velocities at the same epoch, our results are in agreement with these studies.

In summary, regardless of how violent the environment of VINTERGATAN is, reduced depletion times indicating starbursts (~100

Myr) are only achieved once a galactic disc is in place. In our simulation, this starts at $z \approx 4.8$, when $v_{\rm rot,g}/\sigma_{\rm g} > 1$. Later ($z < 1$), in the absence of mergers to compress the ISM and rapidly enhance the SFR, our galaxy grows in size by a factor of ~5 (Paper I), and its depletion time increases to ~few Gyr.

4 DISCUSSION & CONCLUSION

Using the VINTERGATAN cosmological zoom-in simulation (Paper I; Paper II; Paper III), we identify three phases of star formation along the evolution of a Milky Way-type galaxy, consistent with the star formation relations derived from observations:

a) Early on ($z > 4.8$, 12.7 Gyr ago), the gas depletion time in VINTERGATAN is long (~1 Gyr) despite the ubiquity of mergers in this epoch. Interactions prevent the galaxy from developing a well-ordered morphology and kinematics, maintaining a turbulence level of $\sigma_{\rm g} \sim 10-20\,{\rm km\,s^{-1}}$ in the cold gas. Hence, our small ($R_{1/2} \approx 400$ pc), gas-rich ($f_{\rm g} \gg 50\%$) galaxy has a non-bursty star formation, with rates below ~$10\,{\rm M_\odot\,yr^{-1}}$.

b) At redshifts $1 < z < 4.8$, the kinematics of the cold gas indicate that the structure of the ISM shifts towards coherent motions dominating over turbulent ones ($v_{\rm rot,g} > \sigma_{\rm g}$). Then, during interaction and merger events, gas is compressed on galactic scales, creating an excess at high densities and a tenfold drop of the depletion time (~100 Myr). VINTERGATAN jumps to the starburst sequence in the KS plane (Daddi et al. 2010b), and is also consistent with outliers observed above the MS (Rodighiero et al. 2011; Tacconi et al. 2018) with peaks of SFR $\gtrsim 40\,{\rm M_\odot\,yr^{-1}}$.

c) Starburst events come to an end after the last major merger ($z < 1$, 7.8 Gyr ago), with depletion times rising back to $1-2$ Gyr. In the absence of merger-driven perturbations, the ISM does not maintain its excess of dense gas and the galaxy transitions back to the disc regime in the KS plane (Daddi et al. 2010a; Kennicutt & Evans 2012). The galaxy settles into a massive ($M_\star \approx 10^{11}\,{\rm M_\odot}$), extended ($R_{1/2} \approx 3$ kpc), and rotationally-supported ($v_{\rm rot,g}/\sigma_{\rm g} > 10$) disc, with a relatively quiescent SFR $\approx 10\,{\rm M_\odot\,yr^{-1}}$. This characterises the secular phase of star formation for the last 8 Gyr, placing VINTERGATAN on the main-sequence (Whitaker et al. 2012; Speagle et al. 2014; Schreiber et al. 2015).

Different modes of star formation have also been identified in previous simulations, but without a description of their evolution across cosmic time (i.e. without cosmological context, Renaud et al. 2014, 2019b; Li et al. 2022). Nevertheless, when mimicking high-redshift conditions, idealised simulations of gas-rich, clumpy galaxy mergers report no significant enhancement of star formation (Perret et al. 2014; Fensch et al. 2017). A possible interpretation for such an inefficiency is that the intrinsically high velocity dispersion of the gas in gas-rich discs ($\approx 40\,{\rm km\,s^{-1}}$) saturates during interactions, and thus cannot lead to further compression (Fensch et al. 2017). However, similar levels of turbulence are found in VINTERGATAN at $1 < z < 5$, yet allowing merger-triggered starbursts. Therefore, the discrepancy seen in the star formation response to mergers likely originates from the cosmological context. We suspect that repeated interactions (only present in cosmological setups) could inhibit the formation of massive clumps, or tidally disrupt them, modifying the structure of the galaxies between idealised and cosmological runs.

A similar outcome is also found in the idealised merger simulations of Hopkins et al. (2013), with $f_{\rm gas} = 50\%$, but with massive clumps rapidly dispersed with the adopted implementation of stellar feedback. Using the same feedback model as in VINTERGATAN, simulations of isolated discs show that gas fractions $\gtrsim 20\%$ allow for the formation of long-lived massive clumps (Renaud et al. 2021c; van Donkelaar et al. 2022). Yet, the absence of such clumps in VINTERGATAN indicates that the morphology of the ISM could be a decisive factor for merger-driven starbursts, even after the formation of the disc.

This confirms conclusions from recent infrared observations of galaxies (Hogan et al. 2022) and the analysis of metal-poor stellar populations in the Milky Way (Conroy et al. 2022), which have highlighted the role of disc morphologies and kinematics in influencing the star formation properties along the assembly of galaxies. Future surveys of high redshift sources (JWST, Evans et al. 2022) will help disentangling the complex interplay of mechanisms at stake, and the their evolution across cosmic time.

DATA AVAILABILITY

The data underlying this article will be shared on reasonable request to the corresponding author.

REFERENCES

Agertz O., Kravtsov A. V., 2015, ApJ, 804, 18
Agertz O., Kravtsov A. V., 2016, ApJ, 824, 79
Agertz O., Kravtsov A. V., Leitner S. N., Gnedin N. Y., 2013, ApJ, 770, 25
Agertz O., et al., 2021, MNRAS, 503, 5826
Bigiel F., Leroy A., Walter F., Brinks E., de Blok W. J. G., Madore B., Thornley M. D., 2008, AJ, 136, 2846
Birkin J. E., et al., 2021, MNRAS, 501, 3926
Bolatto A. D., Wolfire M., Leroy A. K., 2013, ARA&A, 51, 207
Bothwell M. S., Kennicutt R. C., Lee J. C., 2009, MNRAS, 400, 154
Bouché N., et al., 2007, ApJ, 671, 303
Brinchmann J., Charlot S., White S. D. M., Tremonti C., Kauffmann G., Heckman T., Brinkmann J., 2004, MNRAS, 351, 1151
Conroy C., et al., 2022, arXiv e-prints, p. arXiv:2204.02989
Daddi E., et al., 2010a, ApJ, 713, 686
Daddi E., et al., 2010b, ApJ, 714, L118
Dekel A., Ginzburg O., Jiang F., Freundlich J., Lapiner S., Ceverino D., Primack J., 2020, MNRAS, 493, 4126
Duncan K., et al., 2019, ApJ, 876, 110
Elbaz D., et al., 2007, A&A, 468, 33
Elbaz D., et al., 2011, A&A, 533, A119
Evans T. A., Fattahi A., Deason A. J., Frenk C. S., 2022, arXiv e-prints, p. arXiv:2204.01794
Fakhouri O., Ma C.-P., Boylan-Kolchin M., 2010, MNRAS, 406, 2267
Federrath C., Roman-Duval J., Klessen R. S., Schmidt W., Mac Low M. M., 2010, A&A, 512, A81
Fensch J., et al., 2017, MNRAS, 465, 1934

Fraser-McKelvie A., et al., 2021, MNRAS, 503, 4992

Fraternali F., Karim A., Magnelli B., Gómez-Guijarro C., Jiménez-Andrade E. F., Posses A. C., 2021, A&A, 647, A194

Genzel R., et al., 2010, MNRAS, 407, 2091

Genzel R., et al., 2015, ApJ, 800, 20

Gómez-Guijarro C., et al., 2022, arXiv e-prints, p. arXiv:2201.02633

Haardt F., Madau P., 1996, ApJ, 461, 20

Hahn O., Abel T., 2011, MNRAS, 415, 2101

Hani M. H., Gosain H., Ellison S. L., Patton D. R., Torrey P., 2020, MNRAS, 493, 3716

Hogan L., et al., 2022, arXiv e-prints, p. arXiv:2202.10576

Hopkins P. F., Cox T. J., Hernquist L., Narayanan D., Hayward C. C., Murray N., 2013, MNRAS, 430, 1901

Hopkins P. F., Kereš D., Oñorbe J., Faucher-Giguère C.-A., Quataert E., Murray N., Bullock J. S., 2014, MNRAS, 445, 581

Hopkins P. F., et al., 2018, MNRAS, 480, 800

Huško F., Lacey C. G., Baugh C. M., 2022, MNRAS, 509, 5918

Jones G. C., et al., 2021, MNRAS, 507, 3540

Kassin S. A., et al., 2012, ApJ, 758, 106

Keel W. C., Kennicutt R. C. J., Hummel E., van der Hulst J. M., 1985, AJ, 90, 708

Kennicutt Robert C. J., 1998, ApJ, 498, 541

Kennicutt R. C., Evans N. J., 2012, ARA&A, 50, 531

Kim E., et al., 2021, MNRAS, 507, 3113

Kretschmer M., Dekel A., Teyssier R., 2022, MNRAS, 510, 3266

Lang P., et al., 2014, ApJ, 788, 11

Lelli F., Di Teodoro E. M., Fraternali F., Man A. W. S., Zhang Z.-Y., De Breuck C., Davis T. A., Maiolino R., 2021, Science, 371, 713

Leroy A. K., Walter F., Brinks E., Bigiel F., de Blok W. J. G., Madore B., Thornley M. D., 2008, AJ, 136, 2782

Leroy A. K., et al., 2013, AJ, 146, 19

Li H., Vogelsberger M., Bryan G. L., Marinacci F., Sales L. V., Torrey P., 2022, MNRAS, 514, 265

Lotz J. M., Jonsson P., Cox T. J., Croton D., Primack J. R., Somerville R. S., Stewart K., 2011, ApJ, 742, 103

Moreno J., et al., 2021, MNRAS, 503, 3113

Müller J., 2000, Journal of Research of the National Institute of Standards and Technology, 105, 551

Narayanan D., Krumholz M., Ostriker E. C., Hernquist L., 2011, MNRAS, 418, 664

Neeleman M., Prochaska J. X., Kanekar N., Rafelski M., 2020, Nature, 581, 269

Nelson E. J., et al., 2021, MNRAS, 508, 219

Noeske K. G., et al., 2007, ApJ, 660, L43

Osborne C., et al., 2020, ApJ, 902, 77

Padoan P., Haugbølle T., Nordlund Å., 2012, ApJ, 759, L27

Pan H.-A., et al., 2018, ApJ, 868, 132

Perret V., Renaud F., Epinat B., Amram P., Bournaud F., Contini T., Teyssier R., Lambert J. C., 2014, A&A, 562, A1

Puglisi A., et al., 2021, MNRAS, 508, 5217

Renaud F., Boily C. M., Naab T., Theis C., 2009, ApJ, 706, 67

Renaud F., et al., 2013, MNRAS, 436, 1836

Renaud F., Bournaud F., Kraljic K., Duc P. A., 2014, MNRAS, 442, L33

Renaud F., Bournaud F., Daddi E., Weiß A., 2019a, A&A, 621, A104

Renaud F., Bournaud F., Agertz O., Kraljic K., Schinnerer E., Bolatto A., Daddi E., Hughes A., 2019b, A&A, 625, A65

Renaud F., Agertz O., Read J. I., Ryde N., Andersson E. P., Bensby T., Rey M. P., Feuillet D. K., 2021a, MNRAS, 503, 5846

Renaud F., Agertz O., Andersson E. P., Read J. I., Ryde N., Bensby T., Rey M. P., Feuillet D. K., 2021b, MNRAS, 503, 5868

Renaud F., Romeo A. B., Agertz O., 2021c, MNRAS, 508, 352

Rizzo F., Vegetti S., Powell D., Fraternali F., McKean J. P., Stacey H. R., White S. D. M., 2020, Nature, 584, 201

Rizzo F., Vegetti S., Fraternali F., Stacey H. R., Powell D., 2021, MNRAS, 507, 3952

Robertson B. E., Kravtsov A. V., 2008, ApJ, 680, 1083

Rodighiero G., et al., 2011, ApJ, 739, L40

Rodríguez Montero F., Davé R., Wild V., Anglés-Alcázar D., Narayanan D., 2019, MNRAS, 490, 2139

Romano M., et al., 2021, A&A, 653, A111

Rosen A., Bregman J. N., 1995, ApJ, 440, 634

Saintonge A., Catinella B., 2022, arXiv e-prints, p. arXiv:2202.00690

Saintonge A., et al., 2017, ApJS, 233, 22

Sargent M. T., Béthermin M., Daddi E., Elbaz D., 2012, ApJ, 747, L31

Schmidt M., 1959, ApJ, 129, 243

Schreiber C., et al., 2015, A&A, 575, A74

Simons R. C., et al., 2017, ApJ, 843, 46

Sparre M., Springel V., 2016, MNRAS, 462, 2418

Sparre M., et al., 2015, MNRAS, 447, 3548

Sparre M., Hayward C. C., Feldmann R., Faucher-Giguère C.-A., Muratov A. L., Kereš D., Hopkins P. F., 2017, MNRAS, 466, 88

Speagle J. S., Steinhardt C. L., Capak P. L., Silverman J. D., 2014, ApJS, 214, 15

Sutherland R. S., Dopita M. A., 1993, ApJS, 88, 253

Tacconi L. J., et al., 2010, Nature, 463, 781

Tacconi L. J., et al., 2013, ApJ, 768, 74

Tacconi L. J., et al., 2018, ApJ, 853, 179

Tacconi L. J., Genzel R., Sternberg A., 2020, ARA&A, 58, 157

Tamfal T., Mayer L., Quinn T. R., Babul A., Madau P., Capelo P. R., Shen S., Staub M., 2021, arXiv e-prints, p. arXiv:2106.11981

Teyssier R., 2002, A&A, 385, 337

Vilella-Rojo G., et al., 2021, A&A, 650, A68

Vogelsberger M., et al., 2014, MNRAS, 444, 1518

Wang T.-M., et al., 2022, arXiv e-prints, p. arXiv:2201.12070

Whitaker K. E., van Dokkum P. G., Brammer G., Franx M., 2012, ApJ, 754, L29

Whitaker K. E., et al., 2014, ApJ, 795, 104

Wise J. H., Turk M. J., Norman M. L., Abel T., 2012, ApJ, 745, 50

Wisnioski E., et al., 2015, ApJ, 799, 209

Wisnioski E., et al., 2019, ApJ, 886, 124

Wuyts S., et al., 2011, ApJ, 742, 96

van Donkelaar F., Agertz O., Renaud F., 2022, MNRAS, 512, 3806

APPENDIX A: CHANGE IN $\tau_{\rm dep}$ WITH $\alpha_{\rm CO}$

Galaxy interactions can potentially lead to short $\tau_{\rm dep}$ and episodes of enhanced star formation. Feedback injected subsequently can lead to reduced $\alpha_{\rm CO}$ values (e.g. Narayanan et al. 2011; Renaud et al. 2019a). To quantify how this affects $\tau_{\rm dep}$ in the PHIBSS galaxies, we apply the relation from Figure 5 in Renaud et al. (2019a), derived from simulations of mergers in starbursting phase:

$$\alpha'_{\rm CO} = 1.33 \log(t_{\rm dep}/\text{Myr}) + 0.13, \tag{A1}$$

and then recompute the gas mass as $M'_{\rm gas} = \alpha'_{\rm CO} M_{\rm gas}/\alpha_{\rm CO}$. Here $\alpha_{\rm CO}$ is derived from the PHIBSS catalogue, assuming that the CO 1-0 transition was used for every galaxy. We finally obtain the modified depletion time $\tau'_{\rm dep} = M'_{\rm gas}/\text{SFR}$.

Furthermore, while the CO 1-0 line is favoured in the local Universe, observations of high redshift galaxies rely on higher CO transitions, implying different $\alpha_{\rm CO}$ conversion factors. To compare the importance of using different transitions to that of a $\tau_{\rm dep}$-dependent $\alpha_{\rm CO}$, we compute another $\tau_{\rm dep}$, derived from the $\alpha_{\rm CO}$ of the CO 3-2 transition, according to Equation 2 of Tacconi et al. (2018). Without information on the merger phase nor on the CO transition used for each individual galaxy in PHIBSS, we apply this method to all the PHIBSS galaxies.

Figure A1 shows the evolution of the depletion times in VINTERGATAN and the PHIBSS galaxies (as in Figure 3), and adds the comparison with the two corrections described above. Accounting for a $\tau_{\rm dep}$-dependent modification of $\alpha_{\rm CO}$ (dotted black line) provides a better agreement between the observations and VINTERGATAN in
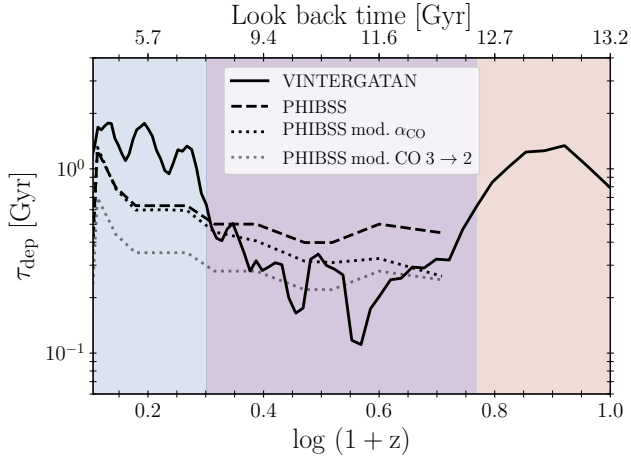
Figure A1. Gas depletion times from VINTERGATAN, compared to three estimates for the PHIBSS galaxies: (*i*) the raw values from the catalogue (as in Figure 3), (*ii*) with an α_{CO} modified to account for the starburst activity (Equation A1, see Renaud et al. 2019a), and (*iii*) with an α_{CO} assuming the use of the CO 3-2 transition for all galaxies.

the *Starburst* stage. A similar effect is found when modifying α_{CO} for the CO 3-2 transition (dotted grey line), although the use of this transition for all galaxies implies an over-correction at low redshift.

In conclusion, modifying α_{CO} to account for the effects of merger-driven starbursts reconciles the depletion time of VINTERGATAN with that of the PHIBSS galaxies at high redshifts.

This paper has been typeset from a TEX/LATEX file prepared by the author.